Supporting Information

Caberlotto et al. 10.1073/pnas.1017114108

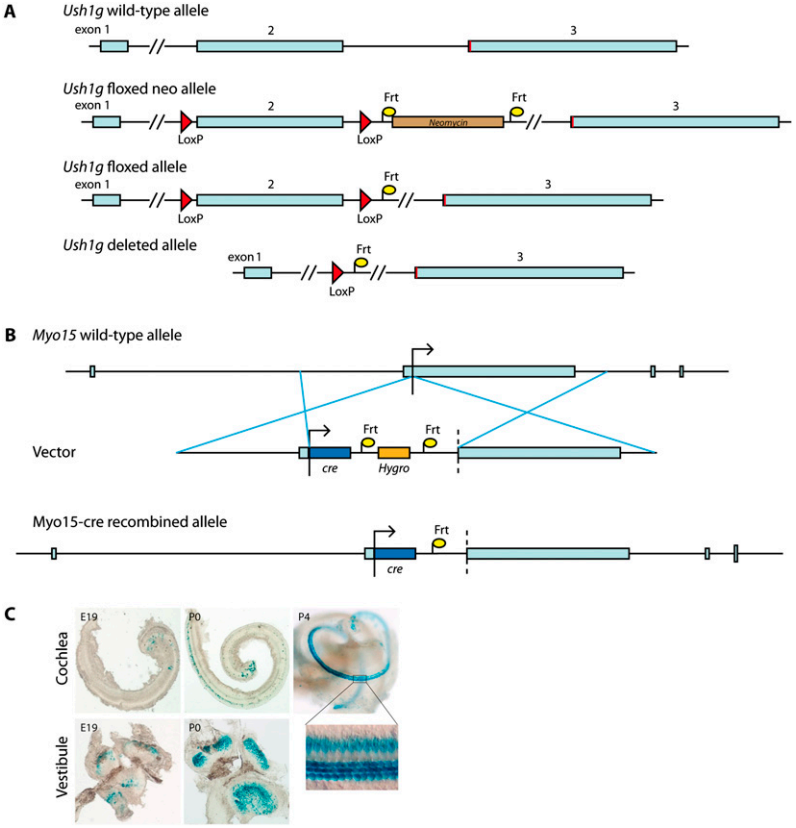

Fig. S1. Engineering of *Ush1g* knockout mice and *Myo15-cre* mice. (*A*) Schematic of the recombinant *Ush1g* alleles. A targeting vector was designed in which *loxP* sites were introduced upstream and downstream of *Ush1g* exon 2, and a neo cassette flanked with *FRT* sites as selectable marker was introduced downstream of exon 2. The targeting construct was electroporated into embryonic stem cells from the 129S1/SvImJ mouse strain, and positive ES cells were selected by their resistance to G418. Stem cells carrying the targeted construct were injected into blastocysts from C57BL/6J mice to obtain chimeric mice. After germline transmission, mice were crossed with C57BL/6J mice producing Flp recombinase to remove the neo cassette. The $Ush1g^{fl/fl}$ mice (MGI:4361359) lack the neo cassette and behave like wild-type ($^{+/+}$) mice. $Ush1g^{fl/fl}$ mice were crossed either with the PGK-Cre^{m} transgenic mouse strain carrying the cre recombinase gene driven by the early acting phosphoglycerate kinase-1 gene promoter or with *Myo15-cre* recombinant mice carrying the cre recombinase gene driven by the myosin-15 gene promoter which, in the inner ear, deletes only the floxed fragment in hair cells. Genotyping of *Ush1g* recombinant animals was carried out by means of two PCR amplifications, using either *oligo-3* (5′-GTCAAAGGATCAGATCACTCGCAG-3′) and *oligo-1* (5′-GGGAGTCGGCTTAACACCACATTG-3′) to detect the wild-type (323-bp amplicon) or floxed (423-bp amplicon) alleles or *oligo-3* and *oligo-4* (5′-CAGTTTCCCCATGTTGATCACCAAC-3′) to detect the presence of a deleted allele lacking *Ush1g* exon 2 (322-bp amplicon). All studies were performed on mixed C57BL/6–129/Sv genetic backgrounds. (*B*) Schematic of the *Myo15-Cre* allele engineered for this study. The cre recombinase gene was placed under the control of the *Myo15* promoter: a targeting construct was designed containing a hygromycin resistance cassette flanked with *FRT* sites and introduced in C57BL/6J mice blastocysts, and after germline transmission, mice were crossed with C57BL/6J mice producing Flp recombinase to remove the hygromycin cassette (MGI:4361284). The heterozygote $Myo15\text{-}cre^{+/-}$ mice behave like wild-type ($^{+/+}$) mice. Genotyping of the animals was done using *Myo15-F* primer (5′-AGGGACCTGACTCCACTTTGGG-3′) with either *Myo15-R* primer (5′-GGAACTGACCTTTCTTAGAGATCTTGGG-3′) to detect the wild-type allele or *cre-R* (5′-TGGTGCACAGTCAGCAGGTTGG-3′) to detect the *Myo15-cre* allele (450-bp amplicon). (*C*) X-Gal staining on $ROSA26^{+/-}Myo15\text{-}cre^{+/-}$ mice. The temporal-spatial expression pattern of *cre* driven by the *Myo15* promoter in the inner ear was assessed by crossing $Myo15\text{-}cre^{+/-}$ mice with ROSA26-lacZ reporter mice (1). The cre-driven *lacZ* expression was studied in the inner ear of $ROSA26^{+/-}Myo15\text{-}cre^{+/-}$ mice using X-Gal histochemistry. *LacZ* expression was first detected in vestibular hair cells at E19, and in hair cells from the cochlear base at P0. At P4, *lacZ* expression was detected in all cochlear hair cells.

1. Soriano P (1999) Generalized lacZ expression with the ROSA26 Cre reporter strain. *Nat Genet* 21:70–71.

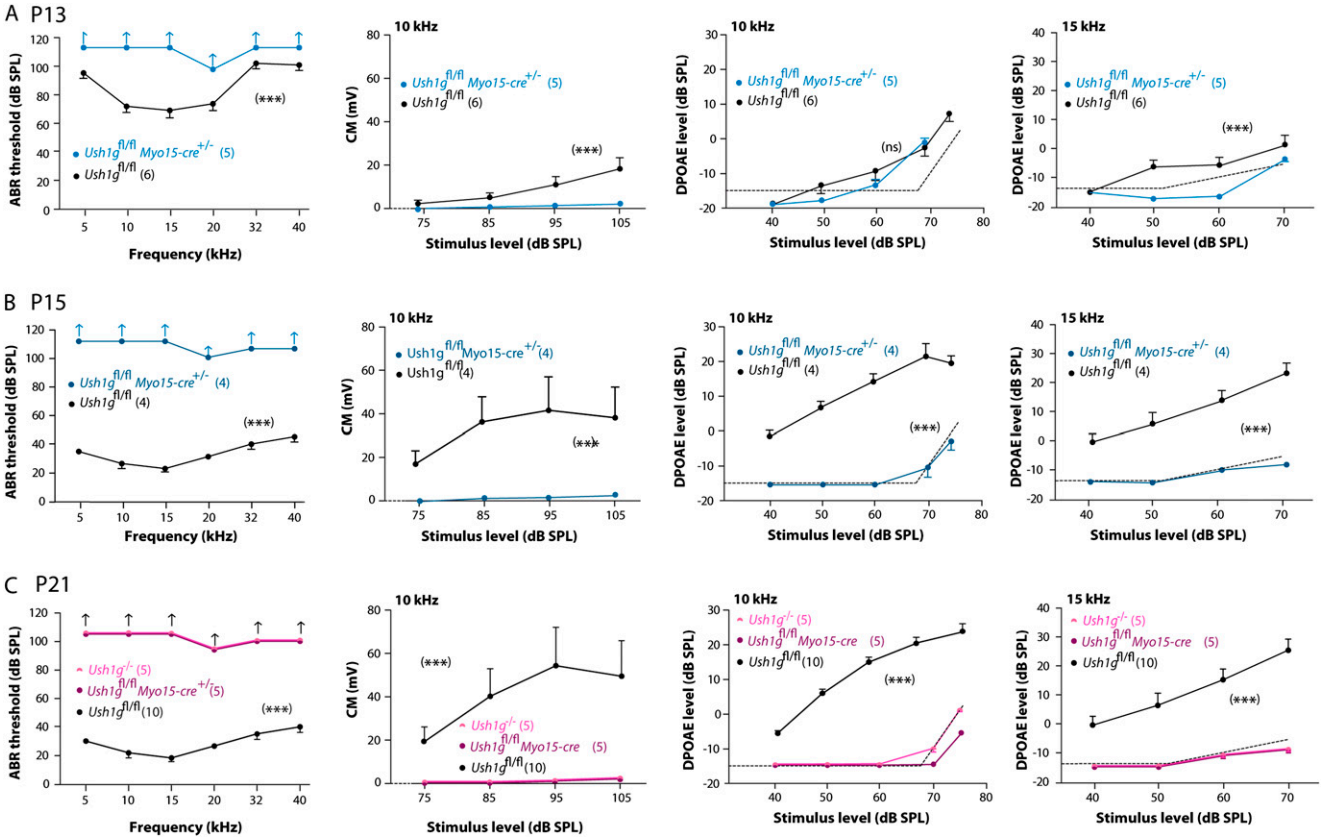

Fig. S2. Analysis of the auditory function in *Ush1g*$^{fl/fl}$*Myo15-cre*$^{+/-}$ P13, P15, and P21 mice and in *Ush1g*$^{-/-}$ P21 mice. (*A*, first graph) Auditory brainstem response (ABR) thresholds (mean ± SEM) in *Ush1g*$^{fl/fl}$ (black line) and *Ush1g*$^{fl/fl}$*Myo15-cre*$^{+/-}$ (blue line) P13 mice for 5- to 40-kHz tone bursts. *Ush1g*$^{fl/fl}$*Myo15-cre*$^{+/-}$ mutants show a total absence of evoked response (two-way ANOVA, $P < 10^{-3}$). (second graph) Growth functions of cochlear microphonics (CM) (mean ± SEM) at increasing stimulus level from 75 to 105 dB for *Ush1g*$^{fl/fl}$ mice and from 90 to 100 dB for *Ush1g*$^{fl/fl}$*Myo15-cre*$^{+/-}$ mice. (third and fourth graphs) DPOAE amplitude (mean ± SEM) at frequency $2f_1 - f_2$ for f_2 = 10 kHz and f_2 = 15 kHz in *Ush1g*$^{fl/fl}$ and *Ush1g*$^{fl/fl}$*Myo15-cre*$^{+/-}$ P13 mice. The DPOAE amplitude was recorded in response to two equal-level primary tones, f_1 and f_2, with f_2/f_1 = 1.20. Cubic DPOAEs were elicited by a CubeDis system (Mimosa Acoustics, v2.43). Frequency f_2 was swept at one-tenth-octave steps from 4 to 20 kHz (levels increased stepwise from 30 to 70 dB SPL). For f_2 = 10 kHz, *Ush1g*$^{fl/fl}$*Myo15-cre*$^{+/-}$ mice show detectable DPOAEs for stimulus level from 60 to 70 dB, whereas no DPOAEs are detected for f_2 = 15 kHz. (*B*, first graph) ABR thresholds (mean ± SEM) in *Ush1g*$^{fl/fl}$ (black line) and *Ush1g*$^{fl/fl}$*Myo15-cre*$^{+/-}$ (blue line) P15 mice for 5- to 40-kHz tone bursts. *Ush1g*$^{fl/fl}$*Myo15-cre*$^{+/-}$ mutants show a total absence of evoked response (two-way ANOVA, $P < 10^{-3}$). (second graph) Growth functions of CM (mean ± SEM) at an increasing stimulus level from 75 to 105 dB for *Ush1g*$^{fl/fl}$ mice and from 90 to 100 dB for *Ush1g*$^{fl/fl}$*Myo15-cre*$^{+/-}$ mice. (third and fourth graphs) DPOAE amplitude (mean ± SEM) at frequency $2f_1 - f_2$ (f_1/f_2 = 1.20) for f_2 = 10 kHz and f_2 = 15 kHz in *Ush1g*$^{fl/fl}$ and *Ush1g*$^{fl/fl}$*Myo15-cre*$^{+/-}$ P15 mice. *Ush1g*$^{fl/fl}$*Myo15-cre*$^{+/-}$ mice have no detectable DPOAEs. (*C*, first graph) ABR thresholds (mean ± SEM) in *Ush1g*$^{fl/fl}$ (black lines), *Ush1g*$^{-/-}$ (pink line), and *Ush1g*$^{fl/fl}$*Myo15-cre*$^{+/-}$ (purple line) P21 mice for 5- to 40-kHz tone bursts. *Ush1g*$^{-/-}$ and *Ush1g*$^{fl/fl}$*Myo15-cre*$^{+/-}$ mutants show a total absence of evoked response (two-way ANOVA, $P < 10^{-3}$). (second graph) Growth functions of CM (mean ± SEM at an increasing stimulus level from 75 to 105 dB. (third and fourth graphs) DPOAE amplitude (mean ± SEM) at frequency $2f_1 - f_2$ (f_1/f_2 = 1.20) in *Ush1g*$^{fl/fl}$, *Ush1g*$^{-/-}$, and *Ush1g*$^{fl/fl}$*Myo15-cre*$^{+/-}$ P21 mice. *Ush1g*$^{-/-}$ and *Ush1g*$^{fl/fl}$*Myo15-cre*$^{+/-}$ mice have no detectable DPOAEs. Dashed line represents noise floor below 65 dB SPL and instrumental distortion above 65 dB SPL.

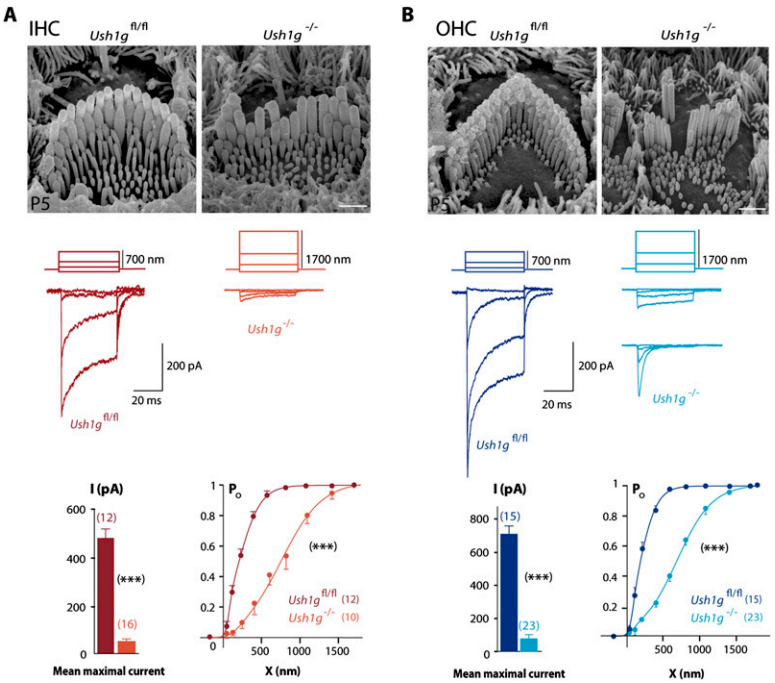

Fig. S3. Hair cell morphology and mechanoelectrical transduction current recordings in inner hair cells (IHCs) and outer hair cells (OHCs) from *Ush1g*$^{-/-}$ P5 mice. (*A*, *Top*) scanning electron microscopy analysis of IHCs from *Ush1g*$^{fl/fl}$ and *Ush1g*$^{-/-}$ P5 mice. (Scale bar: 1 μm.) In *Ush1g*$^{-/-}$ IHCs, some stereocilia of the second row (about 10%) have a prolate end shape, which suggests that some tip-links are still present. Note the reduced length of most stereocilia from the small and medium rows. (*Middle*) Examples of transduction current recordings in an *Ush1g*$^{fl/fl}$ IHC (*Left* panel in dark-red) and an *Ush1g*$^{-/-}$ IHC from P5 mice while applying different displacement steps with a glass probe in the excitatory direction and a 150-nm step in the inhibitory direction (calibrated voltage command of the stimulator at the top). (*Bottom*) Mean maximum transduction currents and $P_o(X)$ curves plotted for *Ush1g*$^{fl/fl}$ and *Ush1g*$^{-/-}$ P5 mice. The maximal amplitudes of the transduction current are 51 ± 9 pA and 471 ± 40 pA in *Ush1g*$^{-/-}$ and *Ush1g*$^{fl/fl}$ IHCs, respectively (unpaired *t* test, $P < 10^{-4}$). The averaged sensitivity of the transduction currents to hair bundle displacement in the mutant IHCs is 0.99 ± 0.09 μm^{-1} and 2.80 ± 0.15 μm^{-1} in *Ush1g*$^{-/-}$ and *Ush1g*$^{fl/fl}$ IHCs, respectively (unpaired *t* test, $P < 10^{-4}$). $X_{0.5}$ is 745 ± 59 nm and 217 ± 20 nm in *Ush1g*$^{-/-}$ and *Ush1g*$^{fl/fl}$ IHCs, respectively (unpaired *t* test, $P < 10^{-3}$). (*B*, *Top*) Scanning electron microscopy analysis of OHCs from *Ush1g*$^{fl/fl}$ and *Ush1g*$^{-/-}$ P5 mice. Note the fragmented aspect of the hair bundles and the reduced length of most stereocilia from the small and medium rows. However, one can recognize the stereocilia of the first row and some stereocilia of the second row. (Scale bar: 1 μm.) (*Middle*) Examples of transduction current recordings in a *Ush1g*$^{fl/fl}$ OHC and two *Ush1g*$^{-/-}$ OHCs from P5 mice. (*Bottom*) Mean maximum transduction currents and $P_o(X)$ curves plotted for *Ush1g*$^{fl/fl}$ and *Ush1g*$^{-/-}$ P5 mice. The maximal amplitudes of the transduction current are 91 ± 24 pA and 696 ± 50 pA in *Ush1g*$^{-/-}$ and *Ush1g*$^{fl/fl}$ OHCs, respectively (unpaired *t* test, $P < 10^{-3}$). The averaged sensitivity values are 1.51 ± 0.24 μm^{-1} and 2.85 ± 0.26 μm^{-1} in *Ush1g*$^{-/-}$ and *Ush1g*$^{fl/fl}$ OHCs, respectively (unpaired *t* test, $P < 10^{-4}$). In addition, $X_{0.5}$ is 765 ± 63 nm and 202 ± 17 nm in *Ush1g*$^{-/-}$ and *Ush1g*$^{fl/fl}$ OHCs, respectively (unpaired *t* test, $P < 10^{-4}$).

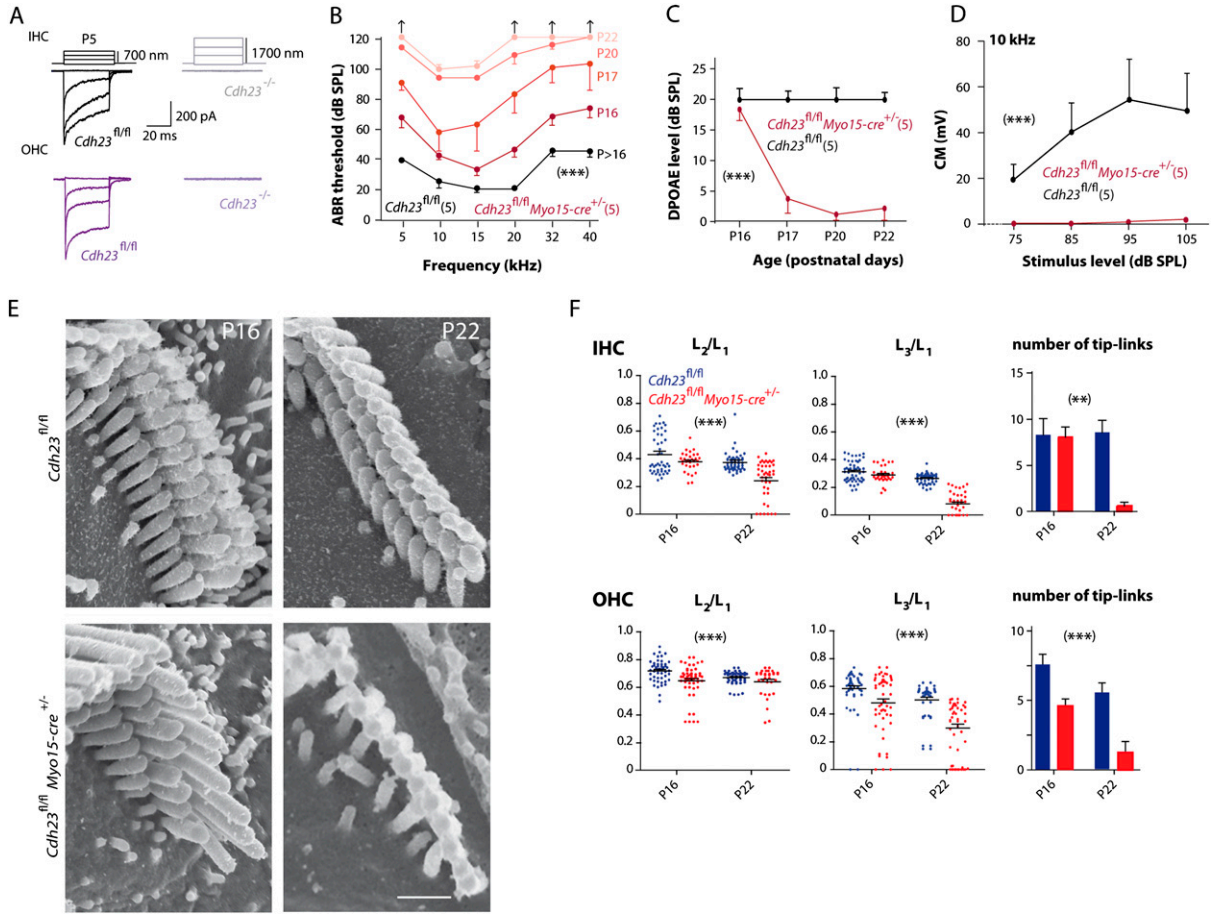

Fig. S4. (*A*) Mechanoelectrical transduction current recordings in inner hair cells (IHCs) and outer hair cells (OHCs) from *Cdh23*$^{fl/fl}$ and *Cdh23*$^{-/-}$ P5 mice. Examples of transduction currents in IHCs (*Upper*) and OHCs (*Lower*) from *Cdh23*$^{fl/fl}$ and *Cdh23*$^{-/-}$ P5 mice in response to a 40-ms mechanical stimulation of the hair bundle. No current is recorded in the *Cdh23*$^{-/-}$ IHC (gray) and OHC (light purple). (*B–D*) Analysis of the auditory function in *Cdh23*$^{fl/fl}$*Myo15-cre*$^{+/-}$ mice at P16, P17, P20, and P22. (*B*) Auditory brainstem response (ABR) thresholds in *Cdh23*$^{fl/fl}$ (black lines) and *Cdh23*$^{fl/fl}$*Myo15-cre*$^{+/-}$ (red lines) P16–P22 mice for 5- to 40-kHz tone bursts (mean ± SEM). *Cdh23*$^{fl/fl}$*Myo15-cre*$^{+/-}$ mutants show progressive hearing loss from P16 to P22 and have profound hearing impairment at P22 (two-way ANOVA, $P < 10^{-4}$). (*C*) Amplitude of the distortion-product otoacoustic emissions (DPOAE) (mean ± SEM) recorded at frequency $2f_1 - f_2$ for a 60-dB SPL two-tone stimulus ($f_1/f_2 = 1.20$) in *Cdh23*$^{fl/fl}$ and *Cdh23*$^{fl/fl}$*Myo15-cre*$^{+/-}$ P16, P17, P20, and P22 mice. *Cdh23*$^{fl/fl}$*Myo15-cre*$^{+/-}$ mice have no detectable DPOAE at P22. (*D*) Growth functions of cochlear microphonics (CM) (mean ± SEM) at an increasing stimulus level from 75 to 105 dB in *Cdh23*$^{fl/fl}$ and *Cdh23*$^{fl/fl}$*Myo15-cre*$^{+/-}$ P22 mice. (*E*) Hair bundle morphology in *Cdh23*$^{fl/fl}$*Myo15-cre*$^{+/-}$ OHCs. Scanning electron microscopy analysis of OHCs in the mid region of the cochlea from *Cdh23*$^{fl/fl}$ (*Upper*) and *Cdh23*$^{fl/fl}$*Myo15-cre*$^{+/-}$ (*Lower*) P16 and P22 mice. At P16, the hair bundles of *Cdh23*$^{fl/fl}$*Myo15-cre*$^{+/-}$ OHCs are cohesive, but some stereocilia of the small row already have reduced heights. At P22, the reduction of the stereocilia length has dramatically worsened in the small and middle rows, and some of the stereocilia from the small row have even disappeared. Notably, the length of the stereocilia in the tall row is unchanged. (Scale bar: 1 μm.) (*F*) Analysis of stereocilia length in IHCs and OHCs from P16 and P22 *Cdh23*$^{fl/fl}$*Myo15-cre*$^{+/-}$ mice. Data corresponding to *Cdh23*$^{fl/fl}$ and *Cdh23*$^{fl/fl}$*Myo15-cre*$^{+/-}$ mice are indicated in blue and in red, respectively. Five cells were analyzed in each group. The length of every measurable stereocilium from the middle and small rows was normalized to the mean length of stereocilia in the tall row (L_2/L_1 and L_3/L_1, respectively; mean ± SEM). The numbers (mean ± SEM) of tip-links detected are indicated by histograms (*Right* panels). In both *Cdh23*$^{fl/fl}$*Myo15-cre*$^{+/-}$ IHCs (*Upper* panels) and OHCs (*Lower* panels), there is a progressive reduction of the stereocilia length and a parallel decrease of the number of tip-links detected, compared with *Cdh23*$^{fl/fl}$ IHCs and OHCs (two-way ANOVA, $P < 10^{-2}$ for all comparisons). In *Cdh23*$^{fl/fl}$*Myo15-cre*$^{+/-}$ P22 mice, note that some stereocilia have completely disappeared in both IHCs and OHCs (red dots on the *x* axis), specifically, 18% of stereocilia from the middle row, 36% from the small row in IHCs, and 32% of stereocilia from the small row in OHCs.

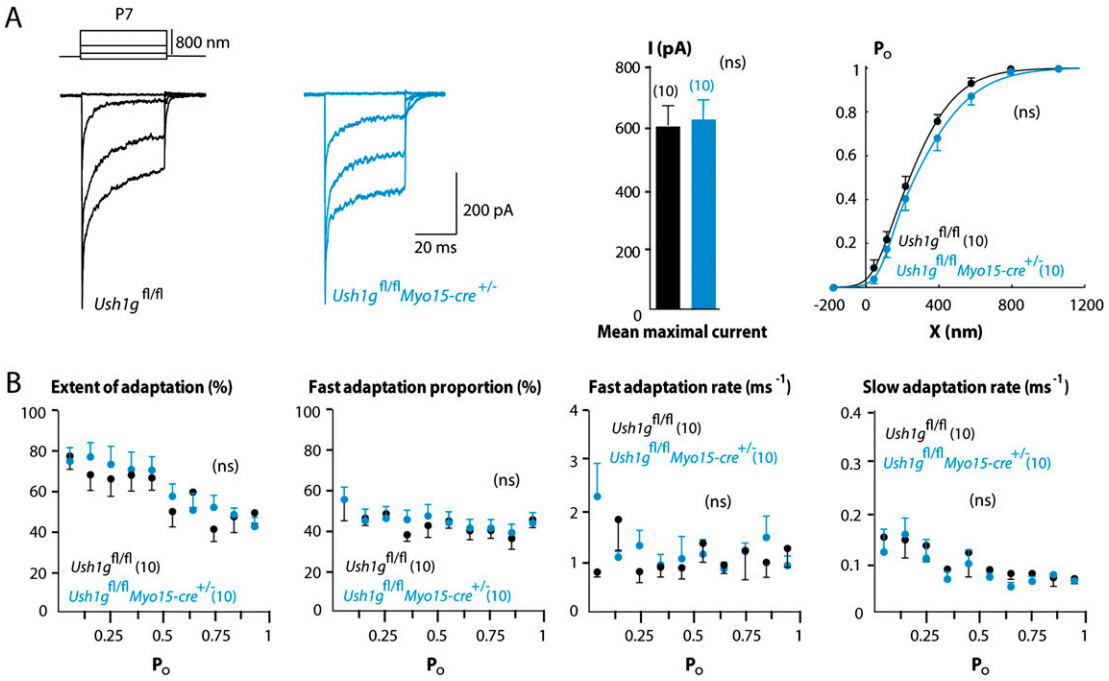

Fig. S5. Analysis of mechanoelectrical transduction current adaptation in inner hair cells (IHCs) from *Ush1g*$^{fl/fl}$*Myo15-cre*$^{+/-}$ P7 mice. Mechanoelectrical transduction currents in cochlear hair cells from the region that is ~40% of the total length of the cochlea from the apex. (*A*) Examples of transduction currents in midcochlear IHCs from *Ush1g*$^{fl/fl}$ (black) and *Ush1g*$^{fl/fl}$*Myo15-cre*$^{+/-}$ (blue) P7 mice. Mean maximum current amplitude is 616 ± 67 pA and 664 ± 71 pA for *Ush1g*$^{fl/fl}$ and *Ush1g*$^{fl/fl}$*Myo15-cre*$^{+/-}$ IHCs, respectively (unpaired *t* test, $P = 0.63$). The $P_o(X)$ curves can be superimposed with values of averaged sensitivity 2.03 ± 0.10 μm^{-1} and 1.85 ± 0.14 μm^{-1} for *Ush1g*$^{fl/fl}$ and *Ush1g*$^{fl/fl}$*Myo15-cre*$^{+/-}$, respectively (unpaired *t* test, $P = 0.35$). In addition, no change in $X_{0.5}$ could be detected in the mutant IHCs with values 248 ± 23 nm and 273 ± 34 nm in *Ush1g*$^{fl/fl}$ and *Ush1g*$^{fl/fl}$*Myo15-cre*$^{+/-}$, respectively (unpaired *t* test, $P = 0.55$). (*B*) We characterized the adaptation in *Ush1g*$^{fl/fl}$ and *Ush1g*$^{fl/fl}$*Myo15-cre*$^{+/-}$ IHCs in terms of its extent and kinetics. The adaptive decline of the transduction current *I* as a function of time *t* was fitted by the double exponential relation $I(t) = A_F\{exp(-(t - t_0)/\tau_F)\} + A_S\{exp(-(t - t_0)/\tau_S)\} + A_{SS}$. In this equation, t_0 is the time at which the stimulus was applied, the fast and slow components of adaptation are characterized by their magnitudes, A_F and A_S, and time constants, τ_F and τ_S, respectively, and A_{SS} describes the transduction current at steady state. From the fit, we deduced the fast and slow adaptation rates, $1/\tau_F$ and $1/\tau_S$, and the proportions, $A_F/(A_F + A_S)$ and $A_S/(A_F + A_S)$, respectively, as well as the extent of adaptation $1 - A_{SS}/(A_F + A_S + A_{SS})$ (1). Statistical significance was tested by using either two-way analysis of variance coupled to the Bonferroni posttest (two-way ANOVA) or two-tailed unpaired *t* test with Welch's correction using the Prism software (GraphPad). We compared the extent of adaptation, the fast adaptation proportion, and the fast and slow adaptation rates in *Ush1g*$^{fl/fl}$ and *Ush1g*$^{fl/fl}$*Myo15-cre*$^{+/-}$ mice, and no change could be detected in the mutant IHCs (two-way ANOVA, $P = 0.34$, $P = 0.60$, $P = 0.42$, and $P = 0.17$, respectively).

1. Kennedy HJ, Evans MG, Crawford AC, Fettiplace R (2003) Fast adaptation of mechanoelectrical transducer channels in mammalian cochlear hair cells. *Nat Neurosci* 6:832–836.

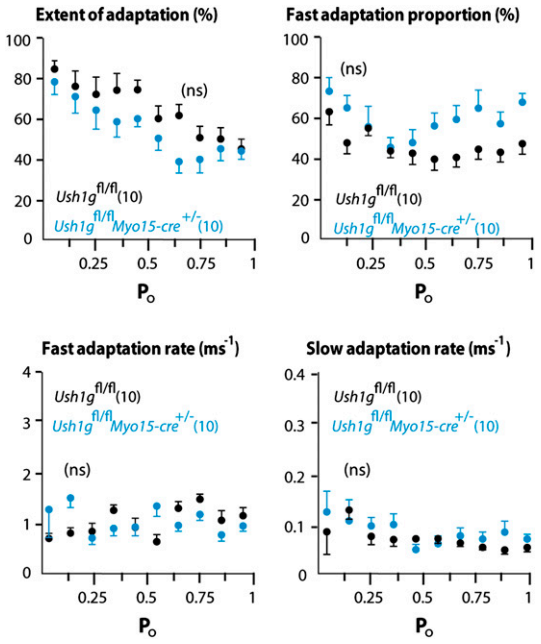

Fig. S6. Analysis of mechanoelectrical transduction current adaptation in *Ush1g*$^{fl/fl}$*Myo15-cre*$^{+/-}$ inner hair cells (IHCs) from the apex. We characterized the adaptation in *Ush1g*$^{fl/fl}$ and *Ush1g*$^{fl/fl}$*Myo15-cre*$^{+/-}$ IHCs from the cochlear apex in terms of its extent and kinetics. The adaptive decline of the transduction current I as a function of time t was fitted by the double exponential relation $I(t) = A_F\{exp(-(t - t_0)/\tau_F)\} + A_S\{exp(-(t - t_0)/\tau_S)\} + A_{SS}$. In this equation, t_0 is the time at which the stimulus was applied; the fast and slow components of adaptation are characterized by their magnitudes, A_F and A_S, and time constants, τ_F and τ_S, respectively; and A_{SS} describes the transduction current at steady state. From the fit, we deduced the fast and slow adaptation rates, $1/\tau_F$ and $1/\tau_S$, and the proportions, $A_F/(A_F + A_S)$ and $A_S/(A_F + A_S)$, respectively, as well as the extent of adaptation $1 - A_{SS}/(A_F + A_S + A_{SS})$ (1). Statistical significance was tested by using either two-way analysis of variance coupled to the Bonferroni posttest (two-way ANOVA) or two-tailed unpaired t test with Welch's correction using the Prism software (GraphPad). We compared the extent of adaptation, the fast adaptation proportion, and the fast and slow adaptation rates in *Ush1g*$^{fl/fl}$ and *Ush1g*$^{fl/fl}$*Myo15-cre*$^{+/-}$ mice, and no change could be detected in the mutant IHCs (two-way ANOVA, $P = 0.78$, $P = 0.44$, $P = 0.08$, and $P = 0.16$, respectively).

1. Kennedy HJ, Evans MG, Crawford AC, Fettiplace R (2003) Fast adaptation of mechanoelectrical transducer channels in mammalian cochlear hair cells. *Nat Neurosci* 6:832–836.

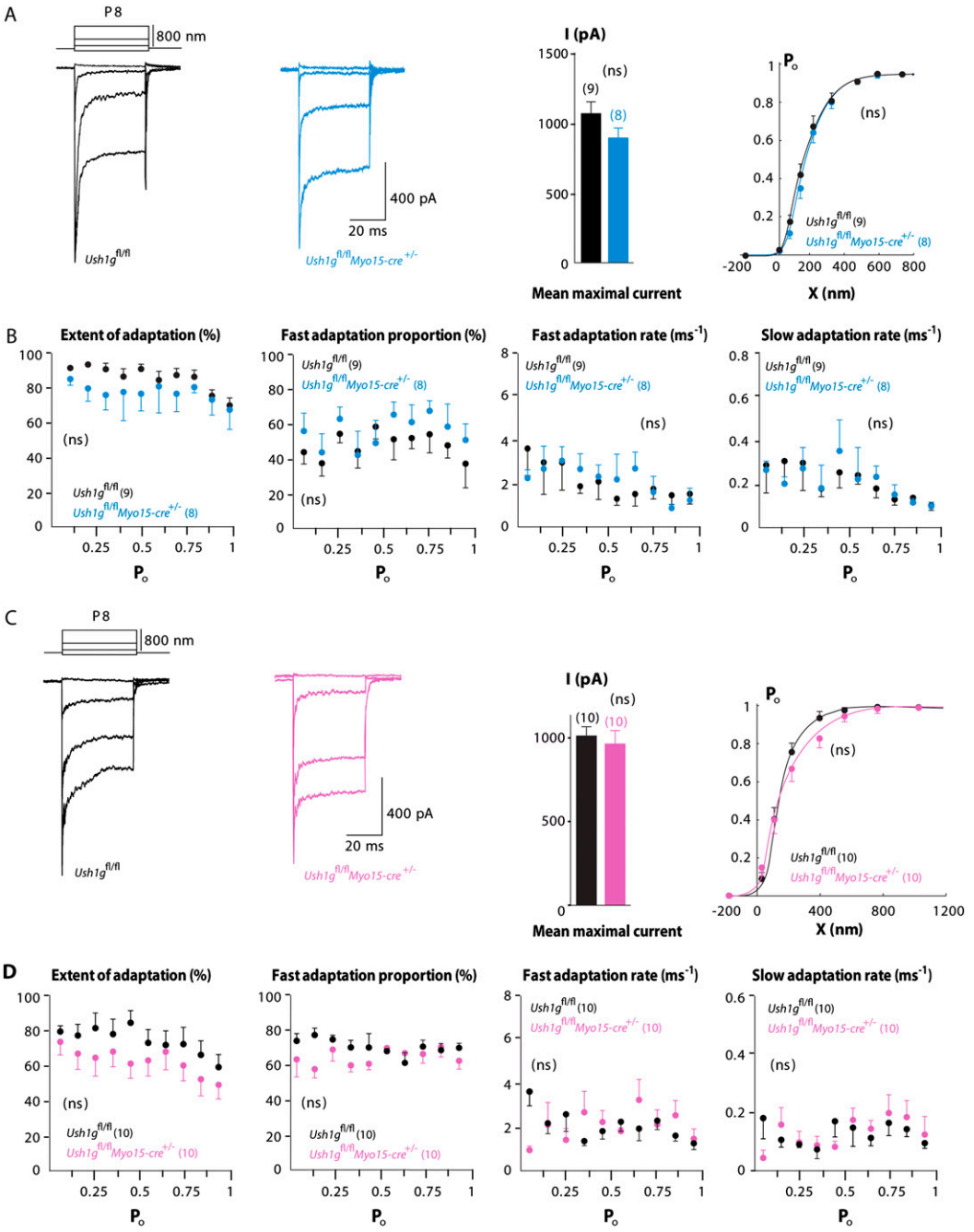

Fig. S7. Mechanoelectrical transduction current recordings in outer hair cells (OHCs) from *Ush1g*$^{fl/fl}$*Myo15-cre*$^{+/-}$ P8 mice. To test if hair cell function was affected despite the absence of morphological changes, we analyzed mechanoelectrical transduction currents at P8 in hair cells from the cochlear apical region (*A* and *B*: ~35% the total length of the cochlea from the apex) and the middle region (*C* and *D*: ~55% the total length) in *Ush1g*$^{fl/fl}$ and *Ush1g*$^{fl/fl}$ *Myo15-cre*$^{+/-}$ mice. (*A*) Examples of transduction currents in apical OHCs from *Ush1g*$^{fl/fl}$ (black) and *Ush1g*$^{fl/fl}$*Myo15-cre*$^{+/-}$ (blue) P8 mice. Mean maximum current amplitude is 1,014 ± 82 pA and 866 ± 67 pA for *Ush1g*$^{fl/fl}$ and *Ush1g*$^{fl/fl}$*Myo15-cre*$^{+/-}$ inner hair cells (IHCs), respectively (unpaired *t* test, $P = 0.19$). The $P_o(X)$ curves can be superimposed, with values of averaged sensitivity of 3.89 ± 0.38 μm^{-1} and 3.41 ± 0.18 μm^{-1} for *Ush1g*$^{fl/fl}$ and *Ush1g*$^{fl/fl}$*Myo15-cre*$^{+/-}$, respectively (unpaired *t* test, $P = 0.28$). In addition, no change in $X_{0.5}$ could be detected in the mutant OHCs, with values of 188 ± 23 nm and 196 ± 12 nm in *Ush1g*$^{fl/fl}$ and *Ush1g*$^{fl/fl}$*Myo15-cre*$^{+/-}$, respectively (unpaired *t* test, $P = 0.9$). (*B*) We characterized the adaptation in *Ush1g*$^{fl/fl}$ and *Ush1g*$^{fl/fl}$*Myo15-cre*$^{+/-}$ OHCs from the cochlear apex in terms of its extent and kinetics. We compared the extent of adaptation, the fast adaptation proportion, and the fast and slow adaptation rates in *Ush1g*$^{fl/fl}$ and *Ush1g*$^{fl/fl}$*Myo15-cre*$^{+/-}$ mice, and no change could be detected in the mutant OHCs (two-way ANOVA, $P = 0.51$, $P = 0.05$, $P = 0.73$, and $P = 0.96$, respectively). (*C*) Examples of transduction currents in an *Ush1g*$^{fl/fl}$ OHC (black) and an *Ush1g*$^{fl/fl}$*Myo15-cre*$^{+/-}$ OHC (pink) from the middle of the cochlea at P8. Mean maximum current amplitude is 963 ± 91 pA and 1,009 ± 60 pA for *Ush1g*$^{fl/fl}$ and *Ush1g*$^{fl/fl}$*Myo15-cre*$^{+/-}$ OHCs, respectively (unpaired *t* test, $P = 0.69$). The $P_o(X)$ curves can be superimposed with values of sensitivity 3.73 ± 0.27 μm^{-1} and 3.19 ± 0.70 μm^{-1} for *Ush1g*$^{fl/fl}$ and *Ush1g*$^{fl/fl}$*Myo15-cre*$^{+/-}$, respectively (unpaired *t* test, $P = 0.48$). In addition, no change in $X_{0.5}$ could be detected in the mutant IHCs, with values of 179 ± 19 nm and 213 ± 29 nm in *Ush1g*$^{fl/fl}$ and *Ush1g*$^{fl/fl}$*Myo15-cre*$^{+/-}$ IHCs, respectively (unpaired *t* test, $P = 0.34$). (*D*) We characterized the adaptation in *Ush1g*$^{fl/fl}$ and *Ush1g*$^{fl/fl}$*Myo15-cre*$^{+/-}$ OHCs from the middle in terms of its extent and kinetics. We compared the extent of adaptation, the fast adaptation proportion and the fast and slow adaptation rates in *Ush1g*$^{fl/fl}$ and *Ush1g*$^{fl/fl}$*Myo15-cre*$^{+/-}$ mice, and no change could be detected in the mutant OHCs (two-way ANOVA, $P = 0.5$, $P = 0.05$, $P = 0.91$, and $P = 0.96$, respectively).

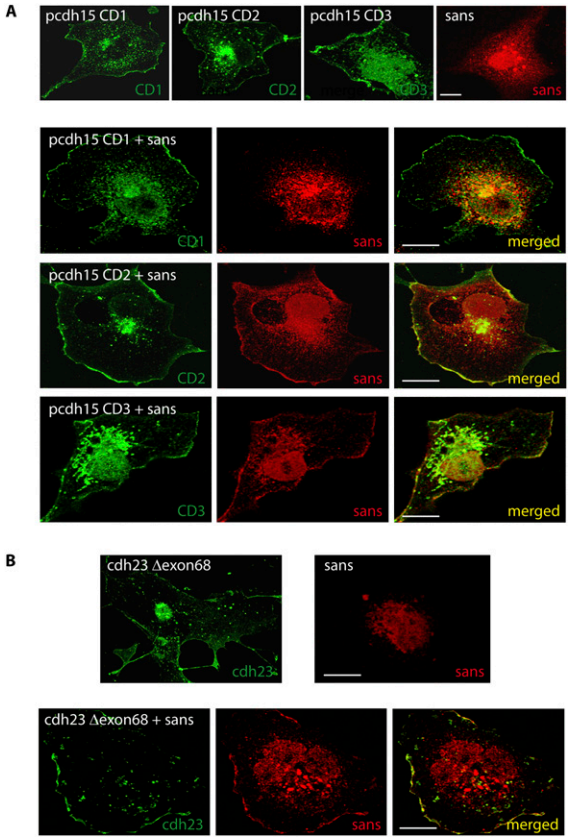

Fig. S8. Protocadherin-15 CD2 and CD3 and cadherin-23 colocalize with sans at the plasma membrane in cotransfected COS-7 cells. (*A*) COS-7 cells were transiently transfected to produce one of the protocadherin-15 (pcdh15) CD1, CD2, or CD3 isoforms and/or sans. In the single-transfected cells, protocadherin-15 CD1, CD2, and CD3, but not sans, are targeted to the plasma membrane. In cotransfected cells, sans is recruited at the plasma membrane only in cells that also produce protocadherin-15 CD2 or CD3, but not CD1. (*B*) COS-7 cells were transiently transfected to produce cadherin-23 (cdh23) and/or sans. In co-transfected cells producing sans and cadherin-23, sans is recruited at the plasma membrane, where it colocalizes with cadherin-23. (Scale bars: 5 μm.)